Available online at www.sciencedirect.com
ScienceDirect
International Journal of Heat and Mass Transfer 51 (2008) 2179–2189
International Journal of HEAT and MASS TRANSFER
www.elsevier.com/locate/ijhmt

Simultaneous heat and moisture transfer through a composite supported liquid membrane

Li-Zhi Zhang [a,*], Fu Xiao [b]

[a] Key Laboratory of Enhanced Heat Transfer and Energy Conservation of Education Ministry, School of Chemical and Energy Engineering, South China University of Technology, Guangzhou 510640, China
[b] Department of Building Services Engineering, The Hong Kong Polytechnic University, Hong Kong, China

Received 10 May 2007; received in revised form 2 November 2007
Available online 27 December 2007

Abstract

Composite supported liquid membranes (SLM) are an efficient transfer media to recover heat and moisture from exhaust air due to the high moisture diffusivity in the liquid layer. However, heat transfer has adverse effects on moisture transfer since the water concentration in the LiCl solution decreases at higher temperatures. This study gives a detailed quantitative analysis of these effects. More specifically, simultaneous heat and moisture transfer through a composite supported liquid membrane is modeled. The SLM involved comprises three layers: two hydrophobic porous skin layers and a hydrophilic porous support layer where a layer of LiCl liquid solution is immobilized in the macro and micro pores as the permselective substance. The equations governing the heat mass transport in the microstructures, as well as the transfer of heat and moisture in the air streams adjacent to the membrane, are solved numerically in a coupled way. An experiment has been built to validate the model. The results found that though heat transfer has adverse effects on moisture transfer, in general, the effects on moisture effectiveness are quite limited. The high moisture permeation rates of SLM can be sustained when there is concomitant simultaneous heat transfer.

1. Introduction

Air conditioning in hot and humid environments is an essential requirement for support of daily human activities. For thermal comfort reasons, indoor air conditions around 25 °C temperature and 10 g/kg humidity ratio are the accepted set points. However, the Southern China and other Southeast Asian countries have a long summer season with a daily average temperature of 28.6 °C, and humidity ratio above 17.6 g/kg. Outdoor relative humidity often exceeds 80% continuously for a dozen of days, leading to mildew growth on wall and furniture surfaces, which affects people's life seriously. Consequently, air dehumidification plays a major role in air conditioning industry in these regions. In many of these countries, the energy used to cool and dehumidify the ventilation air ranges from 20% to 40% of the total energy consumption for air conditioning, and can be even higher where 100% fresh air ventilation is required [1], such as kitchen, hospital, factories.

Membrane-based total heat recovery has been accepted as the most efficient way to save energy consumption. According to this concept, a heat exchanger with a membrane core is installed between the incoming fresh air and the outgoing exhaust air. Fresh air and exhaust air exchange sensible heat and moisture simultaneously through the permselective membranes, thus recovering both cool and dryness in summer. Large quantities of the energy needed to condition the fresh air can be saved. In fact, it is estimated that more than 70% of the energy that is needed to cool and dehumidify the fresh air can be saved by this method [2]. The promising energy savings potential has drawn many studies in this topic, both theoretically [3,4] and experimentally [5,6]. However, real commercial applications are still scarce. The reason lies in the fact that moisture diffusivity in a dense solid membrane is very low,

* Corresponding author. Tel./fax: +86 20 87114268.
E-mail address: Lzzhang@scut.edu.cn (L.-Z. Zhang).

0017-9310/$ - see front matter © 2007 Elsevier Ltd. All rights reserved.
doi:10.1016/j.ijheatmasstransfer.2007.11.006

Nomenclature

a	half channel height (m)
b	half channel length and width (m)
C	concentration (kg/m^3)
c_p	specific heat (kJ kg^{-1} K^{-1})
D	diffusivity (m^2/s)
D_h	hydrodynamic diameter (m)
d_p	pore diameter (m)
h	convective heat transfer coefficient (kW m^{-2} K^{-1})
J	emission rate (kg m^{-2} s^{-1})
k	convective mass transfer coefficient (m/s)
Kn	Knudsen number
k_p	Henry coefficient (kg m^{-3} Pa^{-1})
Le	Lewis number
M	molecule weight (kg/mol)
NTU	number of transfer units
Nu	Nusselt number
P	atmospheric pressure (Pa)
q	heat flux (kW m^{-2})
R	gas constant, 8.314 J/(mol K)
Sh	Sherwood number
T	temperature (K)
U	total transfer coefficient (kW m^{-2} K^{-1} for heat and m/s for mass)
u_a	air bulk velocity (m/s)
v	molecular diffusion volume
V	air volumetric flow rate (L/min)
x	coordinate (m)
y	coordinate (m)

Greek symbols

ρ	density (kg/m^3)
η	effectiveness
λ	heat conductivity (W m^{-1} K^{-1})
ω	humidity ratio (kg moisture/kg air)
τ	pore tortuosity
ε	porosity
δ	thickness (μm)

Superscript

*	dimensionless

Subscripts

a	air
e	equivalent, exhaust air
f	fresh air
i	inlet
k	Knudsen
L	latent
lq	liquid solution
o	outlet, ordinary
s	sensible, solid
tot	total
v	vapor
w	liquid water

in the order of 10^{-12}–10^{-13} m^2/s [7,8]. A total heat exchanger with satisfactory moisture exchange effectiveness, say, 0.6, requires a membrane area that is too large to attract the market interests, from both economical and resistance points of view.

In contrast to solid membranes, moisture diffusivity in liquid membranes ($\sim 10^{-9}$ m^2/s [9,10]) is several orders higher than that in solid membranes. Due to this reason and the inherent high selectivity, the composite supported liquid membranes (SLM) have been proposed as an alternative to traditional solid membranes in many industrial areas [11,12]. In the area of ventilation air heat and moisture recovery, a LiCl solution based SLM has been successfully fabricated [13]. In this research, a layer of LiCl liquid solution was immobilized in a porous support membrane to transfer moisture while impeding other unwanted gases like CO_2. To protect the SLM, two hydrophobic PVDF (polyvinylidene fluoride) layers were formed on both surfaces of the SLM. The microscopic view of the membrane structure is shown in Fig. 1. As seen in the figure, there are totally three layers: two PVDF porous skin layers and a porous AC (acetate cellulose) layer which is to support the liquid LiCl solution in its macro and micro pores. The permeation tests show that the moisture permeation rates through such a SLM are two times higher than through solid membranes. With this membrane, the performance of a total heat exchanger can be dramatically improved and the membrane area can be largely decreased, which are the key to market success.

The character of a total heat exchanger is that besides mass transfer, there is concomitant simultaneous heat transfer. It is believed that high temperature will have bad effects on moisture transfer, since water concentration in the LiCl solution, which is the driving force for moisture transfer, will decrease at higher temperatures. The SLM will have little use unless this bad effect can be prevented, or at least controlled. Therefore, simultaneous heat and moisture transfer through the SLM is of interest for the success of a SLM based total heat exchanger. However, a literature review found that though there are many studies involving liquid membranes [14,15], heat transfer is seldom considered. In fact, nearly all previous studies concentrated only on mass transfer, while neglecting heat transfer phenomena. This is the background of this investigation. The difference between this study and author's other published work like Niu and Zhang [4] and Zhang [13] is that Niu and

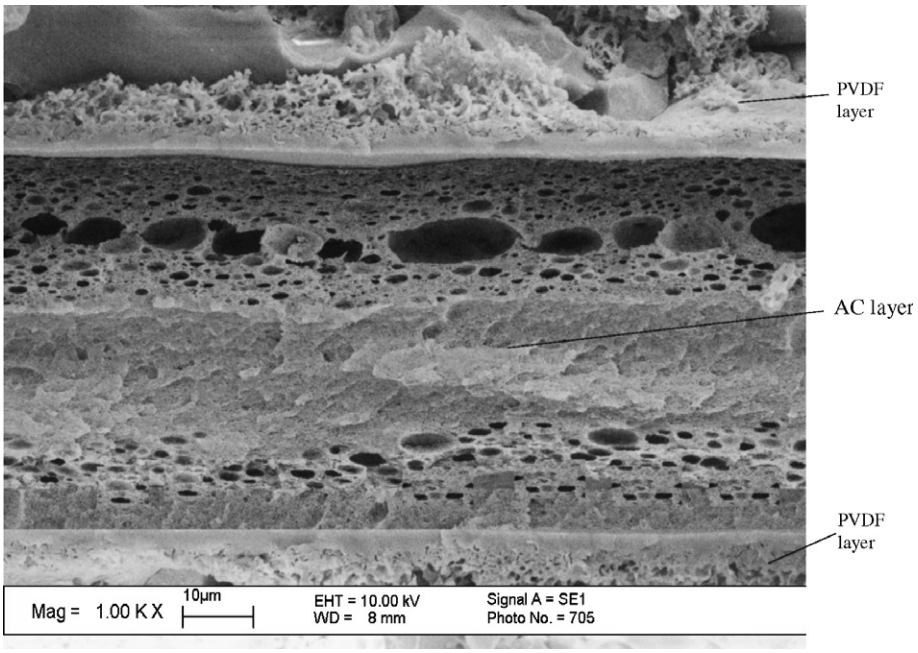

Fig. 1. Microscopic view of cross-section of the composite supported liquid membrane.

Zhang [4] only considers solid membrane, not a supported liquid membrane; while Zhang [13] only considers the isothermal mass transfer in the supported liquid membrane, by neglecting heat transfer. This study is a step forward by considering coupled heat and mass transfer.

2. Experimental work

An experimental set-up has been built to study the simultaneous heat and moisture transport in a SLM based cross-flow total heat exchanger. The membrane was fabricated in the laboratory according to the technique described in Ref. [13]. Its micro structures have been shown in Fig. 1. The whole test set-up is shown in Fig. 2. Ambient air is humidified and is driven to a heating/cooling coil in a hot/cool water bath. The cooling coil can also act as dehumidifier when necessary. After the temperature and humidity reach test conditions, the air is then drawn through the exchanger for heat and moisture exchange. Another flow is driven directly from ambient to the exchanger as the second flow. The composite supported liquid membrane is sandwiched by two stainless steel shell. Two parallel air passages on both sides of membrane are formed, which is like a one-plate plate-and-shell heat exchanger. In the test, a 10 mm thick insulation layer is placed on the inner surface of the shell to prevent heat dissipation from the shell to the surroundings. After the exchanger and pipes are installed, additional insulation is added on the outside surfaces to minimize heat losses from the unit. The exchanger is a cross-flow square one.

The nominal operating conditions: fresh air inlet 35 °C and 0.025 kg/kg; exhaust air inlet 25 °C and 0.010 kg/kg. During the experiment, air flow rate is changed, to have different Reynolds numbers. Humidity, temperature, and volumetric flow rates are monitored at the inlet and outlet of the exchanger. To have a balanced flow, equal air flow

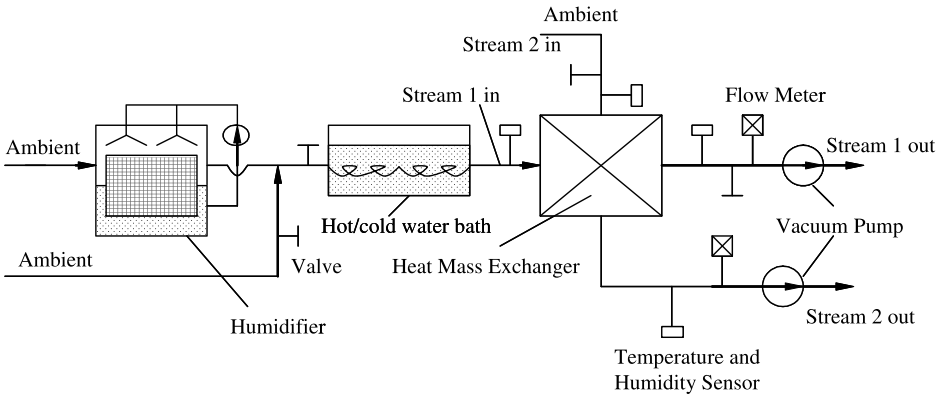

Fig. 2. Experimental set-up.

rates are kept for the two air streams. Volumetric air flow rates are varied from 5 L/min to 35 L/min, corresponding to air velocities from 0.5 m/s to 3 m/s which are typical for commercial total heat exchangers. The uncertainties are: temperature ±0.1 °C; humidity ±2%; volumetric flow rate ±1%. The final uncertainty is ±4.5%.

After the inlet and outlet temperature and humidity are measured, the sensible exchange effectiveness and the latent exchange effectiveness can be calculated for a balanced flow

$$\eta_s = \frac{T_{fi} - T_{fo}}{T_{fi} - T_{ei}} \tag{1}$$

$$\eta_L = \frac{\omega_{fi} - \omega_{fo}}{\omega_{fi} - \omega_{ei}} \tag{2}$$

where T and ω represent temperature (°C) and humidity ratio (kg/kg), respectively; subscripts f and e represent fresh air and exhaust air, respectively; subscripts i and o represent inlet and outlet, respectively. The outlet temperature and humidity could also be calculated from the model described below.

3. Mathematical model

3.1. Composite supported liquid membrane

The flow directions and the coordinates system are shown in Fig. 3. The fresh and the exhaust are arranged in a cross-flow structure due to easiness in duct sealing. The whole membrane is composed of three layers. The heat and moisture transfer through the membrane can be depicted by a model shown in Fig. 4.

Moisture flux through the composite membrane is expressed by

$$J = \rho_a D_e \frac{\omega_1 - \omega_4}{\delta_1 + \delta_2 + \delta_3} \tag{3}$$

where D_e is the effective moisture diffusivity in the composite membrane (m^2/s), it is calculated by

$$D_e = \frac{\delta_1 + \delta_2 + \delta_3}{\frac{\delta_1}{D_{e1}} + \frac{\delta_2}{D_{e2}} + \frac{\delta_3}{D_{e3}}} \tag{4}$$

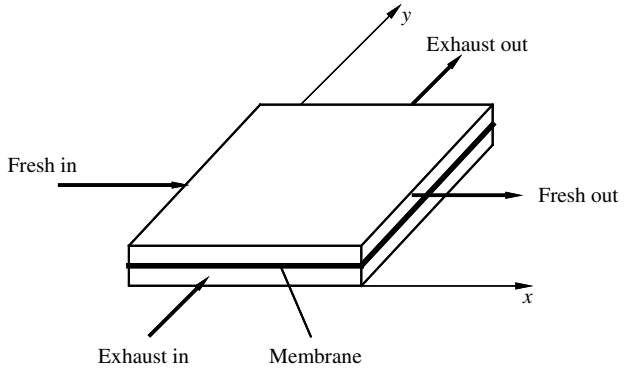

Fig. 3. Arrangements of the flow channels.

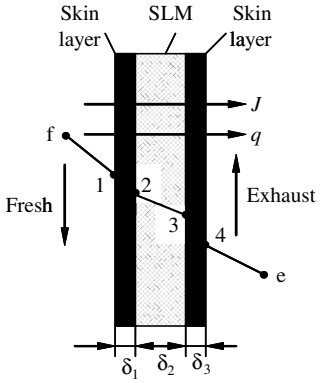

Fig. 4. Heat and mass transfer model in the composite supported liquid membrane.

where D_{e1}, D_{e2}, D_{e3} are the effective diffusivity in the first, second, and third layer, respectively.

The established theory of gas diffusion in hydrophobic membranes considers three mechanisms: Poiseuille flow, ordinary molecular diffusion and Knudsen diffusion, or a combination of them.

When Kn (ratio of the pore size to the mean free path) $\geqslant 10$, the Knudsen flow is dominant, the Poisseuille mechanism may be neglected. Actually, in most cases for air conditioning industry with microporous membranes, Knudsen number is larger than 10, and Poisseuille flow can be neglected, then the flow is considered to be combined Knudsen and ordinary diffusion.

Ordinary diffusion coefficient of water vapor molecule in air is expressed by Tomaszewska et al. [16]

$$D_0 = \frac{C_a T^{1.75}}{P\left(v_v^{1/3} + v_a^{1/3}\right)^2}\sqrt{\frac{1}{M_v} + \frac{1}{M_a}} \tag{5}$$

where $C_a = 3.203 \times 10^{-4}$. The terms v_v and v_a are molecular diffusion volumes and are calculated by summing the atomic contributions [16]. M_v and M_a are molecule weight of vapor and air in kg/mol. P is the atmospheric pressure (Pa)

Knudsen diffusion coefficient [16]

$$D_K = \frac{d_P}{3}\sqrt{\frac{8RT}{\pi M_v}} \tag{6}$$

where R is gas constant, 8.314 J/(mol K); and d_p is mean pore diameter (m). d_p is actually the mean surface pore size. The membrane bulk pore size is compensated by a parameter named tortuosity τ.

The effective diffusivity of combined Knudsen and ordinary flow is [16]

$$D_{KO}^{-1} = \left(D_K^{-1} + D_O^{-1}\right)^{-1} \tag{7}$$

Effective diffusivity in this layer [16]

$$D_{e1} = \frac{\varepsilon_1}{\tau_1} D_{KO} \tag{8}$$

where ε_1 and τ_1 are porosity and tortuosity of the first layer, respectively. The porosity can be determined by an instrument named ASAP (Accelerated Surface Area and Porosimetry system). The big cavities in the AC layer shown in Fig. 1 are not the original pores in membrane. They are resulted from interaction between LiCl solution and AC membrane when the AC membrane is soaked by the solution and some small pores connects and forms bigger cavities. However, when they are completely filled by LiCl solution, these cavities will have little influence on transfer properties, since the liquid phase will form a continuous layer in membrane.

The effective diffusivity in the third layer is the same as the first layer.

Water diffusion in the liquid membrane:

$$J = \frac{\varepsilon_2}{\tau_2} D_{\mathrm{wl}} \frac{C_{\mathrm{w2}} - C_{\mathrm{w3}}}{\delta_2} \tag{9}$$

where D_{wl} is water diffusivity in liquid solution ($\mathrm{m^2/s}$), C_{w} is the water concentration in liquid membrane solution ($\mathrm{kg/m^3}$).

Water vapor partial pressure, temperature, and LiCl solution concentrations are strongly coupled and governed by thermodynamic equations. The relations between the C_{w} and humidity can be summarized by the following linear equation similar to Henry's sorption law as [13]

$$C_{\mathrm{w}} = 1.608 P \omega k_{\mathrm{p}} + C_{\mathrm{w0}} \tag{10}$$

where k_{p} is called the Henry coefficient ($\mathrm{kg\,m^{-3}\,Pa^{-1}}$), and C_{w0} is a constant ($\mathrm{kg/m^3}$). Following correlations can be used to estimate k_{p} and C_{w0} from temperature [13]:

$$k_{\mathrm{p}} = 0.2625 - 0.0093T + 9.0 \times 10^{-5} T^2 \tag{11}$$

$$C_{\mathrm{w0}} = 739.9 - 1.1T \tag{12}$$

The equivalent diffusion coefficient of vapor in liquid membrane is

$$D_{\mathrm{e2}} = \frac{1.608 P k_{\mathrm{p}} \varepsilon_2}{\rho_{\mathrm{a}} \tau_2} D_{\mathrm{wl}} \tag{13}$$

Heat flux through the composite membrane

$$q = \frac{\lambda_{\mathrm{e}}(T_1 - T_4)}{\delta_1 + \delta_2 + \delta_3} \tag{14}$$

$$\lambda_{\mathrm{e}} = \frac{\delta_1 + \delta_2 + \delta_3}{\frac{\delta_1}{\lambda_1} + \frac{\delta_2}{\lambda_2} + \frac{\delta_3}{\lambda_3}} \tag{15}$$

The heat conductivity in the first layer can be analyzed by [17]

$$\lambda_1 = \lambda_{\mathrm{a}} \varepsilon_1 + \lambda_{\mathrm{s}}(1 - \varepsilon_1) \tag{16}$$

where subscripts a and s denote moist air and solid material part, respectively. The effective heat conductivity of the third layer is assumed as the same to the first layer, since they are the same material.

Similarly, the heat conductivity in the second layer, where a liquid solution is stationed in the porous media, can be analyzed by

$$\lambda_2 = \lambda_{\mathrm{lq}} \varepsilon_2 + \lambda_{\mathrm{s}}(1 - \varepsilon_2) \tag{17}$$

where subscripts lq denote liquid solution.

3.2. Air streams

Assumptions: (1) Heat conduction and vapor diffusion of the two air streams along flow directions (axial) are negligible compared to energy transport and vapor convection by bulk flow. (2) Absorption of water vapor and liquid solution is in equilibrium absorption-state.

As depicted in Fig. 5, the two air streams are in cross-flow arrangement. The fresh air flows along x direction. It can be divided laterally (in y direction) into a number of parallel small fluids. For each small fluid, the temperature and humidity change along flow under the following partial differential conservation equations:

$$\frac{\partial T_{\mathrm{f}}^*}{\partial x^*} = \mathrm{NTU}_{\mathrm{sf}}\left(T_1^* - T_{\mathrm{f}}^*\right) \tag{18}$$

$$\frac{\partial \omega_{\mathrm{f}}^*}{\partial x^*} = \mathrm{NTU}_{\mathrm{Lf}}\left(\omega_1^* - \omega_{\mathrm{f}}^*\right) \tag{19}$$

Similarly, for exhaust air:

$$\frac{\partial T_{\mathrm{e}}^*}{\partial y^*} = \mathrm{NTU}_{\mathrm{se}}\left(T_4^* - T_{\mathrm{e}}^*\right) \tag{20}$$

$$\frac{\partial \omega_{\mathrm{e}}^*}{\partial y^*} = NTU_{\mathrm{Le}}\left(\omega_4^* - \omega_{\mathrm{e}}^*\right) \tag{21}$$

The dimensionless temperature and humidity are defined by

$$T^* = \frac{T - T_{\mathrm{ei}}}{T_{\mathrm{fi}} - T_{\mathrm{ei}}} \tag{22}$$

$$\omega^* = \frac{\omega - \omega_{\mathrm{ei}}}{\omega_{\mathrm{fi}} - \omega_{\mathrm{ei}}} \tag{23}$$

The dimensionless coordinates are defined by

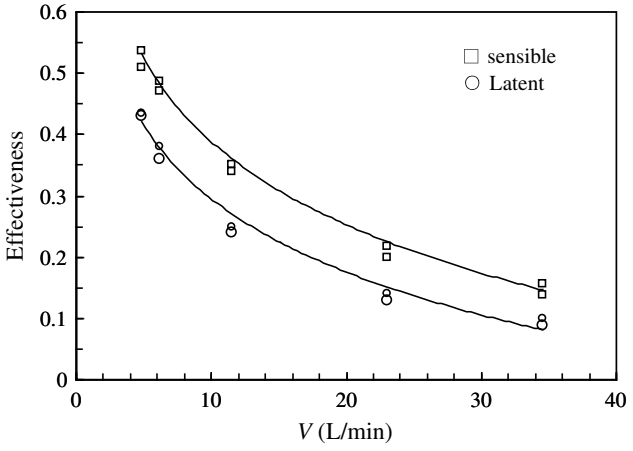

Fig. 5. Sensible and latent effectiveness of the exchanger, discrete dots are the measured values.

$$x^* = \frac{x}{2b} \tag{24}$$

$$y^* = \frac{y}{2b} \tag{25}$$

where b is half channel length (m). The air side number of transfer units for heat and moisture are defined by

$$\mathrm{NTU}_{\mathrm{sf}} = \frac{h_{\mathrm{f}} b}{\rho_{\mathrm{a}} a u_{\mathrm{a}} c_p} \tag{26}$$

$$\mathrm{NTU}_{\mathrm{se}} = \frac{h_{\mathrm{e}} b}{\rho_{\mathrm{a}} a u_{\mathrm{a}} c_p} \tag{27}$$

$$\mathrm{NTU}_{\mathrm{Lf}} = \frac{k_{\mathrm{f}} b}{\rho_{\mathrm{a}} a u_{\mathrm{a}}} \tag{28}$$

$$\mathrm{NTU}_{\mathrm{Le}} = \frac{k_{\mathrm{e}} b}{\rho_{\mathrm{a}} a u_{\mathrm{a}}} \tag{29}$$

where k and h are convective mass transfer coefficient (m/s) and convective heat transfer coefficient ($\mathrm{kW\,m^{-2}\,s^{-1}}$) respectively; u_{a} is air bulk velocity (m/s); a is half channel height (m) and b is half duct width (length) as depicted in Fig. 3.

The final temperature and humidity ratios are determined by the outlet values in air streams governed by (18)–(21). They are measurable parameters. Eq. (3) is just used to get the balance between fresh air and exhaust air at membrane/air interfaces. This is necessary for a detailed distributed model.

The convective heat transfer coefficient and mass transfer coefficient can be calculated by

$$Nu = \frac{hD_{\mathrm{h}}}{\lambda_{\mathrm{a}}} \tag{30}$$

$$Sh = \frac{kD_{\mathrm{h}}}{D_{\mathrm{va}}} \tag{31}$$

where D_{h} is the hydrodynamic diameter (m). For fully developed laminar flow in parallel plates channels, $Nu = 7.54$. The heat and mass transfer coefficients are determined by Eqs. (30)–(32). They are considered as constant since a fully developed laminar flow is realized. Under fully developed laminar flow, the Nu and Sh are constants.

Convective mass transfer can be an analogy to convective heat transfer by [4]

$$Sh = Nu \cdot Le^{-1/3} \tag{32}$$

where Le is the Lewis number, which is 1.12–1.14 for moisture air.

The total number of heat transfer units is

$$\mathrm{NTU}_{\mathrm{s,tot}} = \frac{bU_{\mathrm{s}}}{u_{\mathrm{a}} a \rho_{\mathrm{a}} c_p} \tag{33}$$

where U is the total heat transfer coefficient.

$$U_{\mathrm{s}} = \left[\frac{1}{h_{\mathrm{f}}} + \frac{\delta_1 + \delta_2 + \delta_2}{\lambda_{\mathrm{e}}} + \frac{1}{h_{\mathrm{e}}}\right]^{-1} \tag{34}$$

The term in the middle is the thermal resistance of membrane, which is very small compared to the convective resistance and it can be neglected.

Similar to the definition of total number of transfer units for heat, the total number of transfer units for moisture can be written as

$$\mathrm{NTU}_{\mathrm{L,tot}} = \frac{bU_{\mathrm{L}}}{u_{\mathrm{a}} a} \tag{35}$$

where U_{L} is the total mass transfer coefficient.

$$U_{\mathrm{L}} = \left[\frac{1}{k_{\mathrm{f}}} + \frac{\delta_1}{D_{\mathrm{e}_1}} + \frac{\delta_2}{D_{\mathrm{e}_2}} + \frac{\delta_3}{D_{\mathrm{e}_3}} + \frac{1}{k_{\mathrm{e}}}\right]^{-1} \tag{36}$$

3.3. Boundary conditions

Fresh:

$$T^*_{\mathrm{f}}\big|_{x^*=0} = 1 \tag{37}$$

$$\omega^*_{\mathrm{f}}\big|_{x^*=0} = 1 \tag{38}$$

Exhaust:

$$T^*_{\mathrm{e}}\big|_{y^*=0} = 0 \tag{39}$$

$$\omega^*_{\mathrm{e}}\big|_{y^*=0} = 0 \tag{40}$$

During the process of moisture permeation, the moisture is first absorbed into one side of liquid membrane, releasing heat. Under the driving force of concentration gradients in membrane, the absorbed water is then transported to the other side of membrane, and desorbs while absorbing heat. Due to the small thickness (52 μm), the released heat on fresh air side can be balanced by the absorbed heat on the other side of the membrane, as pointed out in Ref. [4]. The heat and moisture couplings between the air streams and the membrane are:

$$h_{\mathrm{f}}(T_{\mathrm{f}} - T_1) = \frac{\lambda_1}{\delta_1}(T_1 - T_2) \tag{41}$$

$$h_{\mathrm{e}}(T_4 - T_{\mathrm{e}}) = \frac{\lambda_3}{\delta_3}(T_3 - T_4) \tag{42}$$

$$k_{\mathrm{f}}(\omega_{\mathrm{f}} - \omega_1) = \frac{D_{\mathrm{e}_1}}{\delta_1}(\omega_1 - \omega_2) \tag{43}$$

$$k_{\mathrm{e}}(\omega_4 - \omega_{\mathrm{e}}) = \frac{D_{\mathrm{e}_3}}{\delta_3}(\omega_3 - \omega_4) \tag{44}$$

4. Results and discussion

4.1. Numerical solution of the model and validation

Before the numerical solution, a finite difference technique is used to discrete the partial differential equations developed for the air streams. The calculating domain is divided into a number of discrete nodes. Each node represents a control volume. The numbers of the calculating nodes are 50 and 50 in x and y directions, respectively. An upstream differencing scheme is used for two air streams. Since three components: two air streams and the composite SLM membrane, are closely interacted, and temperature and humidity are also related to each other,

Table 1
Parameters used in the test and analysis

Symbol	Unit	Value	Symbol	Unit	Value
δ_1, δ_3	μm	45	ε_1, ε_3		0.60
δ_2	μm	52	ε_2		0.55
d_{p1}, d_{p3}	μm	0.15	τ_1, τ_3		3.0
d_{p2}	μm	0.22	τ_2		3.0
b	mm	50.0	a	mm	1.0
D_{wl}	m^2/s	3×10^{-9}	D_{va}	m^2/s	2.82×10^{-5}
λ_{lq}	$W\,m^{-1}\,K^{-1}$	0.50	λ_s	$W\,m^{-1}\,K^{-1}$	0.36

iterative techniques are needed to solve these equations. When the outlet parameters are obtained, the sensible and latent exchange effectiveness can be calculated with Eqs. (1) and (2). A description of the iterative procedure is as following:

(a) Assume initial temperature and humidity fields in the two streams, Eqs. (18)–(21).
(b) Get the temperature and humidity values on membrane surfaces and inter-layer surfaces 1, 2, 3 and 4, by Eqs. (3)–(17).
(c) Taking the current values of temperature and humidity on membrane surfaces as the default values, get the temperature and humidity profiles in two air streams by solving Eqs. (18)–(21).
(d) Go to (b), until the old values and the newly calculated values of temperature and humidity at all calculating nodes are converged.

After these procedures, all the governing equations are solved simultaneously. To assure the accuracy of the results presented, numerical tests were performed for the duct to determine the effects of the grid size. It indicates that 50×50 grids are adequate (less than 0.1% difference compared with 80×80 grids). The final numerical uncertainty is 0.1%.

The membrane and exchanger properties needed in the calculation are listed in Table 1. The physical properties for LiCl solution are taken from Ref. [18]. The physical properties for the membrane are measured in our laboratory.

The measured sensible and latent effectiveness under various volumetric air flow rates are plotted in Fig. 5 as discrete dots. The calculated values from the above model are plotted in the figure as solid lines. Generally the model predictions are acceptable. The maximum deviations are 10.3% for sensible effectiveness prediction, and 7.8% for latent effectiveness prediction.

4.2. Heat transfer

After the model validation, the temperature and humidity fields in the whole exchanger are calculated for the nominal operating conditions: fresh air inlet 35 °C and 0.025 kg/kg; exhaust air inlet 25 °C and 0.010 kg/kg, air velocity 1 m/s. The dimensionless temperature fields for the two air streams are shown in Figs. 6 and 7. The distributions of heat flux through the composite supported liquid membrane are shown in Fig. 8.

As seen from these figures, the temperature of fresh air decreases along the flow in x direction, while the temperature of the exhaust increases along the flow in y direction. Since the two flows are in cross-flow arrangement, the generated temperature contours are skew to x or y coordinates. The heat flux contours shown in Fig. 8 exhibit large disparities on the membrane surface. The heat flux is the highest on the surface where the two inlets meet, while it is the lowest on surface where the two outlets meet. This character is harmful for the efficient heat exchange between the two flows. If a counter-flow arrangement is used, the heat flux differences on membrane surface can be decreased, thus heat transfer efficiencies can be raised. However, most commercial total heat exchangers still use

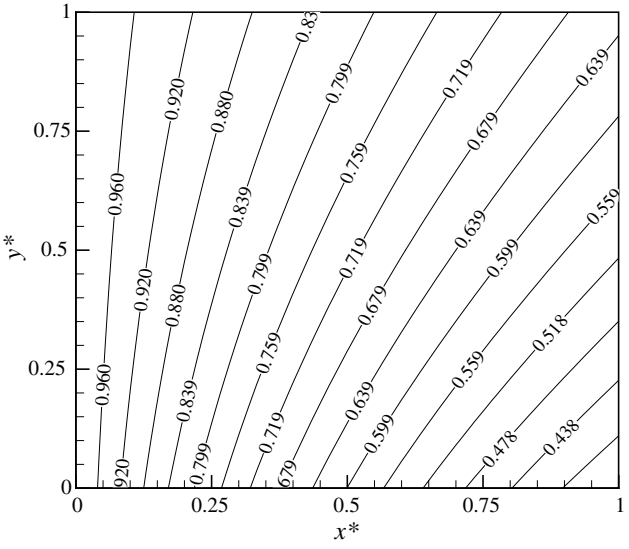

Fig. 6. Dimensionless temperature profiles in fresh air stream.

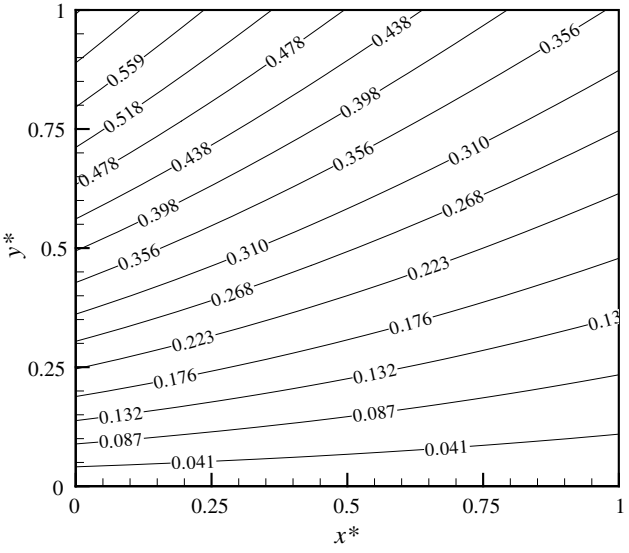

Fig. 7. Dimensionless temperature profiles in exhaust air stream.

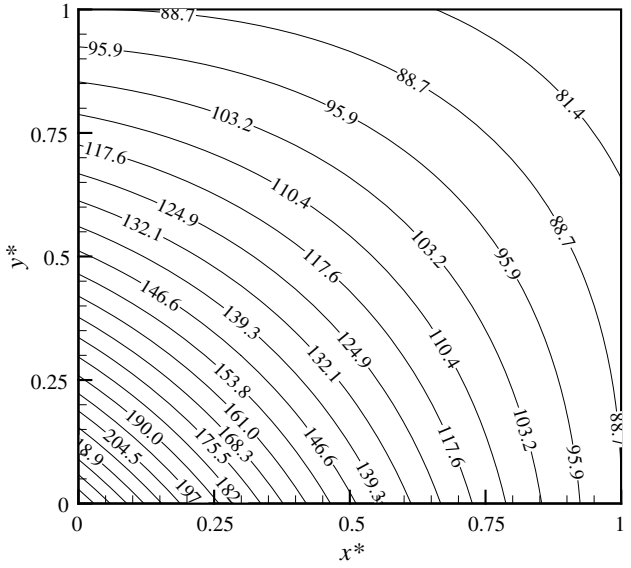

Fig. 8. Heat flux on membrane (W/m^2).

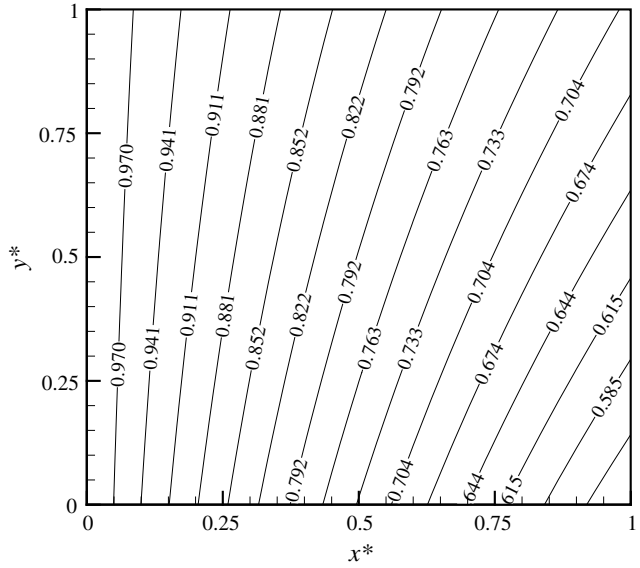

Fig. 10. Dimensionless humidity profiles in fresh air stream.

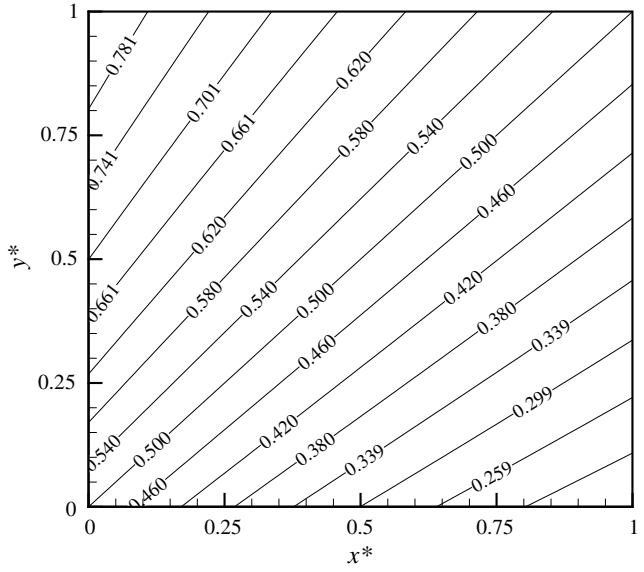

Fig. 9. Contours of the temperature of the membrane.

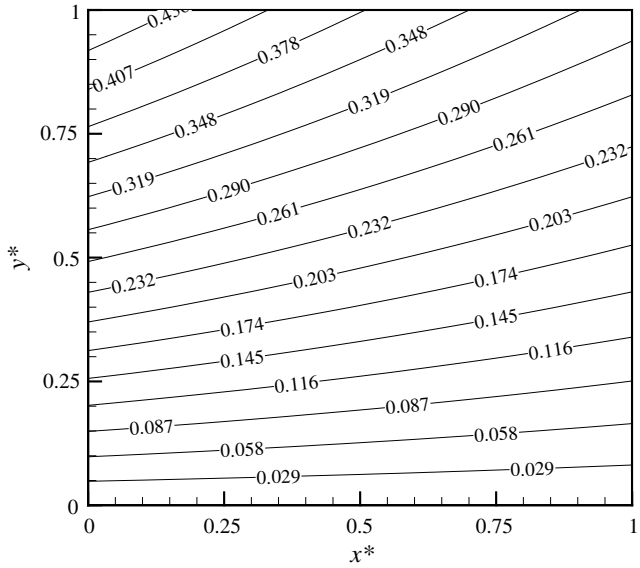

Fig. 11. Dimensionless humidity profiles in exhaust air stream.

cross-flow arrangements due to their simple and convenience in channel sealing and construction.

The contours of the temperature of the membrane are shown in Fig. 9. Due to the small thickness (in the order of 50 μm) of the three layers membrane, the temperature differences between the different layers are negligible. The membrane temperature can be approximated by the average value of the adjacent fresh air and the exhaust air temperatures.

4.3. Moisture transfer

The humidity profiles in the two air streams are shown in Figs. 10 and 11. As seen, the shapes of the dimensionless humidity contours are similar to the temperature contours. The only difference is that the humidity values change along flow in a slower speed, indicating more resistance in the membrane.

The variations of the dimensionless humidity from the fresh air to the exhaust air are shown in Fig. 12 for $x^* = 0$, $x^* = 0.5$, and $x^* = 1$. They are along the same line $y^* = 0.5$. As seen, the slopes of line 23 are the lowest, which indicates that moisture transfer resistance of the liquid layer is the largest one. The lower the slope is, the larger the resistance is. Certainly decreasing the liquid layer thickness could improve the performance further.

The moisture emission rates (mass fluxes) through the membrane are shown in Fig. 13. The shapes are similar

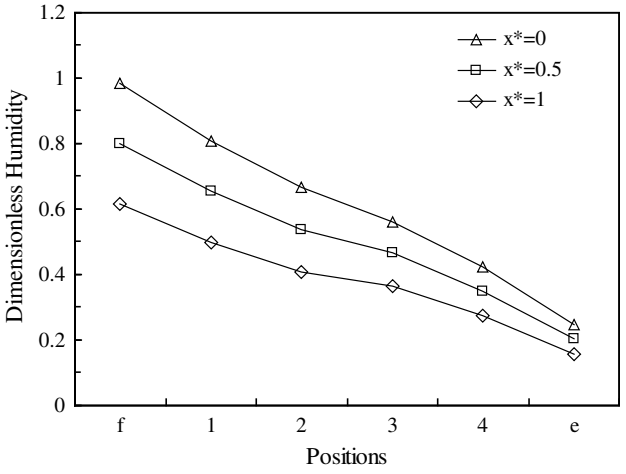

Fig. 12. Variations of dimensionless humidity at $y^* = 0.5$.

to the contours of heat flux: a non-uniform two-dimensional distribution is observed. The emission rates through the SLM are generally greater than 7.0e−5 kg/m^2. In comparison, the average emission rates through a solid hydrophilic polymer membrane in the order of 2.5e−5 kg/m^2 [6]. Therefore, the performance has been greatly improved with a SLM.

The mass ratio of LiCl (kg LiCl/kg solution) in the liquid layer is a function of temperature and humidity. Due to the different air humidity on two sides of the liquid layer, the mass ratio of LiCl on the two sides is different. Figs. 14 and 15 show the contours of the LiCl ratio on fresh air side and exhaust air side, respectively. As observed, both the values and the shapes are different for these two sides. The reason for this phenomenon is that the LiCl concentration is influenced by the temperature and humidity simultaneously. The higher the temperature is, the higher the LiCl concentration is and the lower the water concentration is. The higher the local air humidity is, the lower the LiCl concentration is. The final LiCl concentration is a balance between these contradicting factors. It can be also observed that though the differences between the two sides of the liquid membrane are large (in the order of 0.01), the differences on the same surface is small (in the order of 0.001). Therefore, the LiCl solution concentration can be assumed uniform on a single surface.

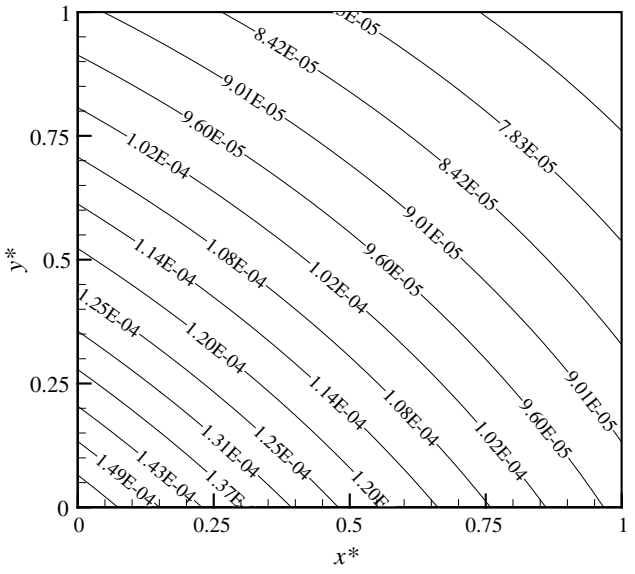

Fig. 13. Emission rate distribution on membrane (kg m^{-2} s^{-1}).

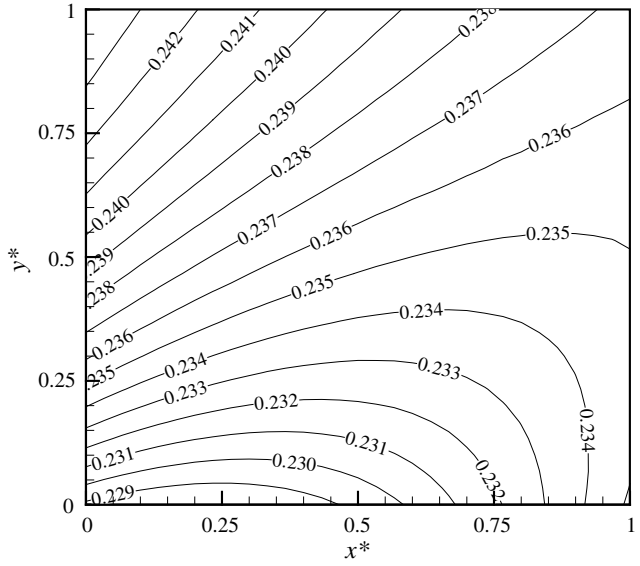

Fig. 14. Mass ratio of LiCl in liquid membrane on fresh air side (kg LiCl/kg solution).

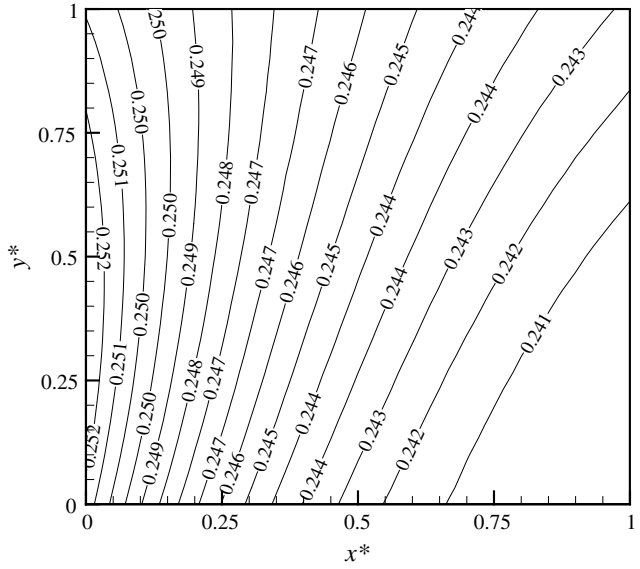

Fig. 15. Mass ratio of LiCl in liquid membrane on exhaust air side (kg LiCl/kg solution).

Heat transfer and moisture transfer are strongly coupled. Table 2 lists the variations of the latent exchange effectiveness with different fresh air inlet temperatures while the other operating conditions are kept unchanged. As

Table 2
Effects of fresh air inlet temperature on latent exchange effectiveness

T_{fi} (°C)	η_L
40	0.385
35	0.389
30	0.393
25	0.396

seen, higher temperatures will have adverse effects on moisture transfer. However, the effects are quite limited. Indeed, when the fresh air inlet temperatures are raised from 25 °C to 40 °C, the latent effectiveness only decreased 3%. Therefore, heat transfer has only limited bad effects on the moisture transfer. The high moisture permeation rates through a SLM that were measured in the isothermal test [13] can be sustained under simultaneous heat and moisture transfer in real applications.

Comparisons between Eqs. (18) and (19), (20) and (21) found that heat transfer and mass transfer equations are in the same forms. Due to this analogy, the traditional effectiveness-NTU method for heat exchanger design also fits for moisture transfer, only if the total number of heat transfer units, $NTU_{s,tot}$, is replaced by the total number of mass transfer units, $NTU_{L,tot}$ [3]. The ratio of $NTU_{L,tot}$ to $NTU_{s,tot}$ for a SLM with 1 m/s air flow speed on both sides is $0.65/1.05 = 0.62$. In extreme cases when the thickness of the two skin layers and the liquid layer is small enough, the $NTU_{L,tot}$ will equal to $NTU_{s,tot}$. In this ideal case, the latent effectiveness will be the same value as the sensible effectiveness.

The supported liquid membrane is rather stable during the experiment, since two porous PVDF membranes are added to protect them. The liquid phase is not lost so replenishment is not needed. In future in real applications, it may lose some amount of liquid phase, then replenishment process is needed. the problem needs further investigation.

5. Conclusions

For a cross-flow heat mass exchanger that uses a composite supported liquid membrane as the transfer media, the temperature and humidity profiles in air streams and on membrane surfaces are numerically obtained by the simultaneous solution of energy and concentration equations of two flows and their couplings with membrane. The model for the membrane takes into account of the micro structure and the mechanisms of heat mass diffusion inside. The results found:

(1) The membrane resistance for heat transfer is negligible, while the resistance for moisture transfer is still substantial.
(2) The LiCl solution concentration can be assumed uniformly distributed on a single surface.
(3) Heat transfer has only limited adverse effects on moisture transfer. The high moisture permeation rates through a SLM that were found in an isothermal test can be sustained under simultaneous heat and moisture transfer in real applications.
(4) Currently, the ratio of $NTU_{L,tot}$ to $NTU_{s,tot}$ for a SLM is around 0.62. When the thickness of the two skin layers and the liquid layer is further decreased, the latent effectiveness will approach the sensible effectiveness.

Acknowledgements

This Project 50676034 is supported by National Natural Science Foundation of China. The project is also partly supported by Program for New Century Excellent Talents in University, NCET-06-0748, and National Key Project of Scientific and Technical Supporting Programs, No. 2006BAA04B02.

References

[1] L.G. Harriman, J. Judge, Dehumidification equipment advances, ASHRAE J. 44 (8) (2002) 22–29.
[2] L.Z. Zhang, J.L. Niu, Energy requirements for conditioning fresh air and the long-term savings with a membrane-based energy recovery ventilator in Hong Kong, Energy 26 (2) (2001) 119–135.
[3] L.Z. Zhang, J.L. Niu, Effectiveness correlations for heat and moisture transfer processes in an enthalpy exchanger with membrane cores, ASME J. Heat Transf. 124 (5) (2002) 922–929.
[4] J.L. Niu, L.Z. Zhang, Membrane-based enthalpy exchanger: material considerations and clarification of moisture resistance, J. Membrane Sci. 189 (2001) 179–191.
[5] K.R. Kistler, E.L. Cussler, Membrane modules for building ventilation, Chem. Eng. Res. & Des. 80 (2002) 53–64.
[6] L.Z. Zhang, Y. Jiang, Heat and mass transfer in a membrane-based energy recovery ventilator, J. Membrane Sci. 163 (1999) 29–38.
[7] C.Y. Pan, C.D. Jensen, C. Bielech, H.W. Habgood, Permeation of water vapor through cellulose triacetate membranes in hollow fiber form, J. Appl. Polymer Sci. 22 (1978) 2307–2323.
[8] F. Debeaufort, A. Voilley, P. Meares, Water vapor permeability and diffusivity through methylcellulose edible films, J. Membrane Sci. 91 (1994) 125–133.
[9] E.L. Cussler, Diffusion-Mass Transfer in Fluid systems, Cambridge University Press, 2000.
[10] C. Isetti, E. Nannei, A. Magrini, On the application of a membrane air–liquid contactor for air dehumidification, Energ. Buildings 15 (1997) 185–193.
[11] A. Sengupta, B. Raghuraman, K.K. Sirkar, Liquid membranes for flue gas desulfurization, J. Membrane Sci. 51 (1990) 105–126.
[12] N.M. Kocherginsky, Q. Yang, L. Seelam, Recent advances in supported liquid membrane technology, J. Membrane Sci. 53 (2007) 171–177.
[13] L.Z. Zhang, Fabrication of a lithium chloride solution based composite supported liquid membrane and its moisture permeation analysis, J. Membrane Sci. 276 (1–2) (2006) 91–100.
[14] A. Alhusseini, A. Ajbar, Mass transfer in supported liquid membranes: a rigorous model, Math. Comput. Model. 32 (2000) 465–480.

[15] R. Fortunato, C.A.M. Afonso, M.A.M. Reis, J.G. Crespo, Supported liquid membranes using ionic liquids: study of stability and transport mechanisms, J. Membrane Sci. 242 (2004) 197–209.
[16] M. Tomaszewska, M. Gryta, A.W. Morawski, Mass transfer of HCl and H_2O across hydrophobic membrane during membrane distillation, J. Membrane Sci. 166 (2000) 149–157.
[17] A.K. Datta, Porous media approaches to studying simultaneous heat and mass transfer in food processes. I: problem formulations, J. Food Eng. 80 (2007) 80–95.
[18] C. Isetti, E. Nannei, A. Magrini, On the application of a membrane air–liquid contactor for air dehumidification, Energ. Buildings 25 (1997) 185–193.